JOM, Vol. 68, No. 9, 2016
DOI: 10.1007/s11837-016-2004-0

The Pivotal Role of Alumina Pore Structure in HF Capture and Fluoride Return in Aluminum Reduction

GRANT J. MCINTOSH,[1,2,4] GORDON E.K. AGBENYEGAH,[1,3] MARGARET M. HYLAND,[1,3] and JAMES B. METSON[1,2]

1.—Light Metals Research Centre, The University of Auckland, Auckland, New Zealand. 2.—School of Chemical Sciences, The University of Auckland, Auckland, New Zealand. 3.—Department of Chemical & Material Engineering, The University of Auckland, Auckland, New Zealand. 4.—e-mail: g.mcintosh@auckland.ac.nz

Fluoride emissions during primary aluminum production are mitigated by dry scrubbing on alumina which, as the metal feedstock, also returns fluoride to the pots. This ensures stable pot operation and maintains process efficiency but requires careful optimization of alumina for both fluoride capture and solubility. The Brunauer-Emmett-Teller (BET) surface area of 70–80 $m^2\ g^{-1}$ is currently accepted. However, this does not account for pore accessibility. We demonstrate using industry-sourced data that pores <3.5 nm are not correlated with fluoride return. Reconstructing alumina pore size distributions (PSDs) following hydrogen fluoride (HF) adsorption shows surface area is not lost by pore diameter shrinkage, but by blocking the internal porosity. However, this alone cannot explain this 3.5 nm threshold. We show this is a consequence of surface diffusion-based inhibition with surface chemistry probably playing an integral role. We advocate new surface area estimates for alumina which account for pore accessibility by explicitly ignoring <3.5 nm pores.

INTRODUCTION

Maintenance of the fluoride balance in an aluminum smelter is extremely important. Fluorides, which form a vital component of the electrolyte, may be lost and emitted to the environment if converted to either volatile particulates or hydrogen fluoride (HF). These compounds are generally toxic.[1–5] Additionally, fluctuations in fluoride level are associated with losses in cell stability and ultimately energy efficiency.[6] These losses are typically compensated for by AlF_3 addition to the cells, but this constitutes a materials input and cost to the smelter.

To close the fluoride balance and reduce the impact of the smelter on the local environment, alumina is used as an HF dry scrubbing agent prior to being fed to the cell for electrolysis. As a consequence of the strength of the Al-F bond, HF binds irreversibly to the alumina surface.[7] It is therefore an excellent medium for scrubbing and fluoride return. Within the smelting community, surface area is typically the parameter by which the efficacy of an alumina as a scrubbing agent is judged: the higher the specific surface area (SSA), the more sites available for gas capture and the more effective the material is presumed to be. The Brunauer-Emmett-Teller (BET) method.[8] is universally employed for SSA determination. While aluminas may achieve SSAs up to $\sim$400 $m^2\ g^{-1}$, balancing other smelter properties has led the consensus to settle on 70–80 $m^2\ g^{-1}$ as a target BET SSA.

However, very little attention has been paid to the microstructure which generates this surface area and the accessibility of the pores which contribute to this. A high SSA material is an ineffective scrubbing agent if much of the porosity cannot be accessed fully on time scales relevant to dry scrubbing. This consideration has been recently been identified by Perander et al.[9,10] who suggest that the finer porosity may be difficult to access. This becomes relevant when it is recognized that the SSA of a material of under- and over-calcined aluminas blended together may have a comparable BET SSA to a more evenly calcined material (so-called bimodal aluminas). However, the blended sample will have a much higher proportion of the porosity associated with these small pores.

(Published online July 13, 2016)

Our alumina group within the Light Metals Research Centre has recently performed a number of studies examining the role of pore size on HF capture efficiency[11,12] and its role in fluoride return to the reduction cells.[13] In this work, we review key elements of these studies, and address the overall implications when these results are taken together. These are supplemented with preliminary results from a model we are currently developing to describe the aging of alumina porosity during reaction with HF. We show that pores smaller than approximately 3.5 nm are not efficiently utilized in fluoride capture during dry scrubbing. In this region of porosity, HF enters a surface diffusion regime that for kinetic reasons inhibits HF from reaching adsorption sites. The mechanism of pore evolution as scrubbing proceeds is also detailed. As a consequence, the universally used BET SSA predictor cannot be used to accurately determine HF scrubbing capacity or fluoride return efficacy. In terms of scrubber performance, there is the potential to introduce a new, more useful SSA predictor to replace this value on alumina specification sheets.

RESULTS

The Impact of Alumina Pore Size on Fluoride Balances in an Operating Smelter

We have correlated several alumina properties with important parameters relevant to smelter operation such as HF generation,[13] current efficiency and energy consumption.[6] In these studies, data from a wide range of smelter parameters were assimilated into 572-point-long vectors, one vector for each parameter. Each data point in a vector represents a daily mean value of that parameter, and was obtained after averaging over 24 h of observation per cell, and further averaged over 60 cells running a common alumina. Each vector is referred to as a predictor. This set of predictors was supplemented with analogous vectors associated with weather conditions (in particular, relative and absolute humidity) and alumina properties (gibbsite and α-Al_2O_3 phase fractions, and SSAs). The collection of vectors less one, the subject of the model, served as the basis for multiple regression analyses where insignificant predictor vectors (at the 95% confidence level) were removed to produce a final multiple regression model. A full overview of model construction is given in Refs. 6 and 13. Studies were performed at TRIMET's Essen smelter employing an injector-type dry scrubber; for the interested reader, full details of the gas treatment centre (GTC) system is provided by Iffert et al.[14]

One of the models of particular relevance to the current work is that of the excess AlF_3 levels of the cell ($XsAlF_3$). It is reasonable to assume that bath fluoride levels should correlate with the surface area of the feed alumina as one of the predictors: the higher the surface area, the greater its ability to capture fluoride and return this to the pots, thereby increasing the $XsAlF_3$ levels. That is, $XsAlF_3$ should exhibit a positive correlation with alumina SSA. However, as the potline ran two different alumina sources concurrently, both competing for fluoride, SSA could not be used directly. Instead, a differential SSA, $\Delta SSA(a)$, was used in recognition of this competitive adsorption, defined as the difference in SSA of concurrently running aluminas a and b, where alumina a is in the end of the potline being studied.

$$\Delta SSA(a) = SSA(b) - SSA(a) \quad (1)$$

With this definition, a negative correlation between $XsAlF_3$ and the surface area predictor is expected.[13]

Surprisingly, using the conventional BET SSA suggests no correlation between surface area and fluoride return with model p values for $\Delta SSA(a) \sim 0.4$. This is well in excess of the ≤ 0.05 threshold required for retention in the final model. However, it has been recognized earlier that the smallest pores may not be readily accessible by HF.[9,10] This porosity, the surface area of which is included in the BET method, can vary considerably between different alumina sources and would therefore introduce a significant amount of noise into the model. Pore size distribution (PSD)-based surface areas were therefore explored. The acronym PSD is also commonly used to refer to particle size distribution. We note that no reference is made to particle size distributions in this work, and PSD refers strictly to the PSD throughout. Each data point in a PSD essentially represents the effective surface area of a representative pore of a given diameter (see Fig. 1). While summing over all pores approximately reproduces the BET SSA, the advantage is that one may restrict the summation to only those pores $\geq x$ nm that may be active in HF capture. These surface areas are denoted as PSD ($\geq x$ nm). All PSDs examined in this work are computed with the Barrett–Joyner–Halenda (BJH) model.[15]

Modeling $XsAlF_3$ levels with PSD ($\geq x$ nm) estimates, initially with $1 \leq x \leq 5$, as the basis of the SSA parameters in Eq. 1 yielded a series of multiple regression models all exhibiting the expected correlation between bath fluoride levels and alumina surface area. This finding indicates that, after such a pore selection to remove the contribution of small pores, a higher surface area alumina indeed returns more fluoride to the cell, and consequently must be removing more HF from the gas streams being released to the environment. It must be noted that SSA does not provide the strongest correlation, with HF generation rates and GTC management playing important, and in some cases dominant, roles. However, the aim of this study is not to produce a holistic model of dry scrubbing operations but rather to extract mechanistic information specifically regarding the role of one particular parameter, alumina quality, on the fluoride balance. Being able

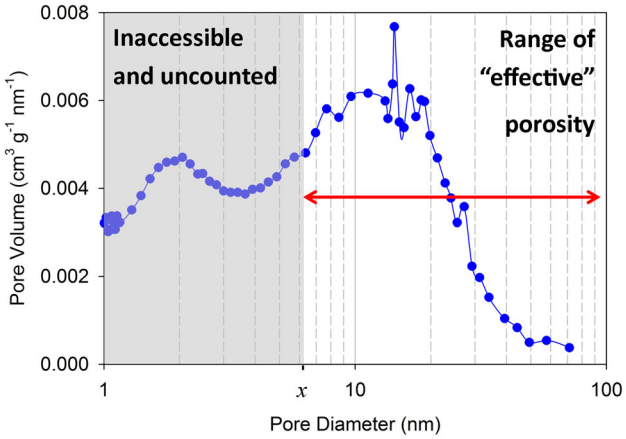

Fig. 1. A typical BJH-based PSD of a bimodal alumina. Total surface areas, determined by summing over all pores, are approximately equal to the BET SSA. Removing the smallest pores (greyed out) from this sum leaves a restricted SSA estimate which omits the noise-introducing fraction. Denoting the smallest retained pore diameter as *x*, this gives the PSD (≥ *x* nm) SSA estimate referred to in this work.

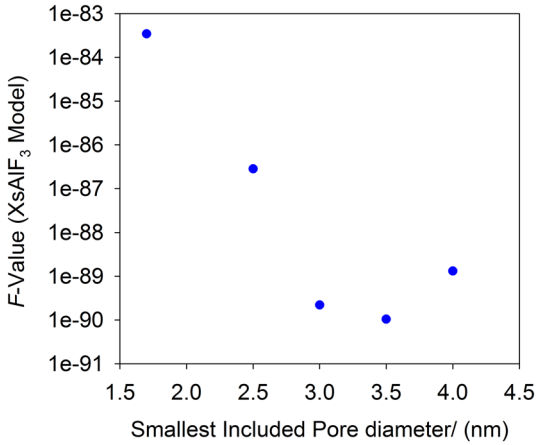

Fig. 2. The overall goodness of fit in the XsAlF$_3$ model as a function of *x* in the PSD (≥ *x* nm) SSA predictor. The smaller the *F* value, the better the model agreement with experiment; note the logarithmic scale on the *y*-axis. This suggests pores smaller than ~3.5 nm are not entirely accessible on the time scales of HF dry scrubbing.

to identify this correlation allows us to probe more deeply into the role of alumina quality on dry scrubbing. Examining the quality of the XsAlF$_3$ regression model as a function of x in the PSD ($\geq x$ nm) predictor, it is possible to explicitly determine the smallest readily accessible pore diameter. The F value, codifying the overall model goodness of fit, is shown in Fig. 2. Starting at ~2 nm, increasing the smallest included pore diameter improves model fitting as this noise-introducing component is removed. An ideal value is reached at $x \sim 3.5$ nm. After this point, model fitting becomes increasing poor again as active porosity is neglected. This provides compelling evidence, based entirely on industry-sourced data, that pores smaller than ~3.5 nm are not wholly accessible to fluoride on time scales relevant to dry scrubbing in injection dry scrubbers of the type used in this study. Consequently, materials in which small pores make a significant contribution to the total surface area, associated with particularly undercalcined aluminas, are not ideal for fluoride capture applications.

PSD Reconstruction Models

In a series of related studies, we have examined changes induced by HF in the PSDs of smelter-grade alumina through carefully controlled laboratory studies. These employ an HF source in a purpose-built dosing apparatus.[11,12] SSA decreases are observed with preferential losses from the smaller pores (typically < 20 nm).[11,12] From this, it is possible to develop a model describing PSD changes and benchmark this against aluminas dosed under both laboratory and industrial conditions.

PSDs effectively provide the total surface area of a pore at a particular pore diameter D_p. If an explicit pore model, typically assuming either cylindrical or slit pore geometries, is adopted, this is sufficient to determine all pertinent geometric parameters of an idealized pore. In particular, an effective pore length, L_p, can be assigned. Perturbation of the pore geometry after assuming a particular model of gas transport and surface area loss provides a powerful tool by which the mechanism of pore aging can be assessed. Note that such manipulations do not make sense with the common BET method. This approach provides a single value for the total surface area and ignores surface geometry entirely. As such, there is no means of extracting any pore diameter dependence.

In deriving this model, we recognized that there are likely several regions of porosity under which unique gas transport phenomena are active. In the largest pores, there is unlikely to be any hindrance to gas mobility. However, as one moves to increasingly narrow pores, limited access on kinetic grounds has been postulated.[9,10] The transition from unhindered access to kinetically restricted porosity, to which unique surface area loss models are to be applied, is not likely to occur abruptly at some threshold pore diameter. Therefore, our model partitions pores according to a gradually varying function that determines the fraction of the length of a pore of a given diameter that should be treated with the each of the adsorption models. An error function (ERF) is assumed for this partitioning:

$$f(D_p) = \frac{1}{2}\left[1 + \mathrm{erf}\left(\frac{D_p - D_{\mathrm{kinetic}}}{\sqrt{2}\sigma_{\mathrm{kinetic}}}\right)\right] \qquad (2)$$

The function $f(D_p)$ represents the fraction of the pore length of diameter D_p that is to be designated as one of the particular sub-pores. Partitioning occurs around a threshold pore diameter D_{kinetic} that represents the point at which exactly half of the pore length is associated with the unrestricted access regime, and half experiences kinetic

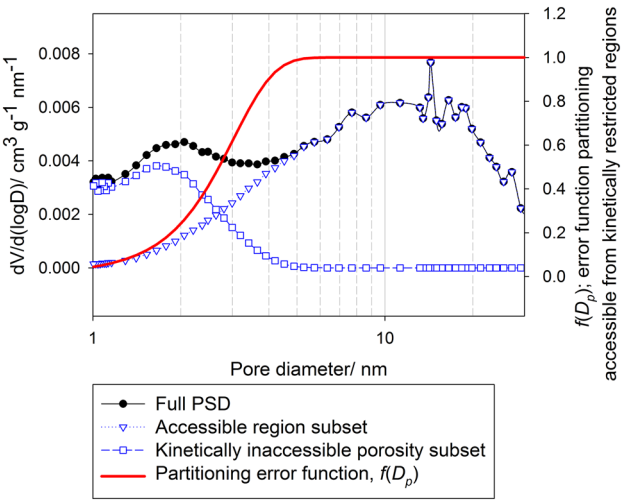

Fig. 3. Pore geometry partioning based on ERFs; see Eq. 2. The ERF splits a particular pore into two, with each subpore set to be treated with different surface area loss models. In the example shown, considering the transition to kinetic inaccessibility, the fraction to the right of the ERF is presumed to exhibit unhindered access, with the remainder completely inaccessible.

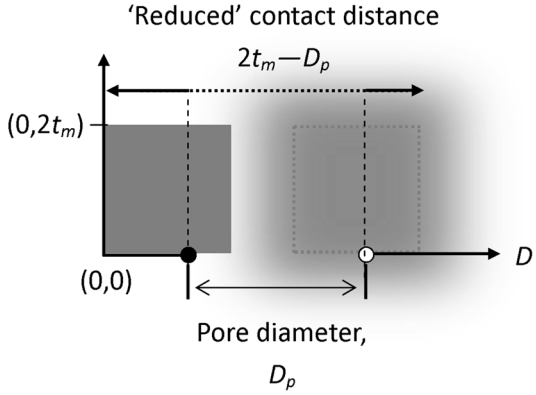

Fig. 4. Schematic presenting the pore blocking model. Formation of a hydroxyfluoride particle, of size t_m, may occur at certain points either side of a pore of diameter D_p. Treating D_p as a discontinuity in the D axis the criteria for blocking requires the far sides of the adsorbate be $2t_m - D_p$ apart, and not $2t_m$ as in Eq. 3. Assuming some uncertainty in the size of the adsorbate or the pore opening diameter, the probability of blocking is determined by summing the probability that the two adsorbate phases touch over all sites the second adsorbate may anchor along the D axis (Eq. 4).

inhibition (see Fig. 3 for an overview). In this model, we assume that kinetic inhibition implies no access to internal porosity. The partition has an associated standard deviation σ_{kinetic}. It is reasonable to expect a smooth transition between these different transport regimes if an interaction with the surface is responsible. This would be expected to become increasingly strong as pore diameter decreases. However, we note that an abrupt change in accessibility at a threshold pore diameter can still be modelled with this approach, if mechanistically reasonable. An abrupt transition would be modelled analogously, but with a Heaviside function with a range of (0,1) in place of an ERF. However, an excellent approximation to this is possible from Eq. 2 in the limit $\sigma_{\text{kinetic}} \rightarrow 0$. Therefore, the ERF will model both scenarios. Further, this exact form of partitioning is assumed to be valid in this instance as concentration profiles under diffusive flow are commonly based on Gaussian distributions.[16,17] This assumes kinetic inhibition is a consequence of diffusion, which is justified later. The ERF is defined as the cumulative probability function (or the integral) of the normal distribution. As such, it is reasonable to assume the probability of an adsorbate entering a section of porosity while moving under diffusive flow will be described by an ERF.

A second partitioning is also hypothesized, valid for smaller porosity again. In this region, adsorption events along the particle's exterior surface produce a hydroxyfluoride product[18–20] of thickness t_m (identified with monolayer thickness in the limit of complete surface coverage) that completely covers the entrance of the pore. As this pore is now blocked to outside ingress, the surface area of affected porosity will be set to zero. While based on fundamentally different physical assumptions, the partitioning of these blocked pores from those kinetically inaccessible can also be shown to depend on ERFs with an analogous interpretation. A schematic from which the underlying equations may be derived is given in Fig. 4. If we assume that one adsorbate phase is positioned at $D = 0$, and the other potentially anywhere else along the surface in the positive D axis direction, the probability that the two adsorbates touch (leading to blocking) if there is no open pore between them is:

$$P_{\text{touch}}(D) = \frac{1}{\sigma_{\text{block}}\sqrt{2\pi}} \exp\left[\frac{-(D-2t_m)^2}{2\sigma_{\text{block}}^2}\right] \quad (3)$$

In this, we assume some normally distributed variability in the adsorbate thickness and/or pore opening, codified by the standard deviation term σ_{block}. Now placing a pore opening of diameter D_p between them, the fractional length of a pore of diameter D_p that is blocked, f_{block} is determined by summing the probability of pore blocking, Eq. 3, over all possible positions the second adsorbate may fix along the D-axis. This is obtained by integrating Eq. 3 over all D:

$$\begin{aligned} f_{\text{block}}(D_p) &= \int_{-\infty}^{\infty} dD P_{\text{touch}}(D) \\ &= 2\int_{-\infty}^{0} dD \frac{1}{\sigma_{\text{block}}\sqrt{2\pi}} \exp\left[\frac{-(D-[2t_m - D_p])}{2\sigma_{\text{block}}^2}\right] \\ &= \left[1 + \text{erf}\left(\frac{2t_m - D_p}{\sqrt{2}\sigma_{\text{block}}}\right)\right] \end{aligned} \quad (4)$$

Note that this has an identical form to Eq. 2 but with different fitting parameters.

With the porosity partitioned appropriately, a model of surface area loss must be applied to each partitioned subset, after which the subpores may be rebinned to give a simulated post-dosing PSD. In the smallest pores, all surface area is set to zero. This is a consequence of porosity being blocked following fluoride exposure. In the middle region, associated with kinetically inhibited access, no model of loss is imposed as it is assumed that HF cannot reach the surface to react.

The mechanism of surface area loss in the largest pores, those exhibiting unrestricted access, is more contentious. It has been previously assumed in the literature concerning HF adsorption by alumina that this occurs by monolayer formation, and therefore effectively by a shrinking core model.[21] Consider for example a cylindrical pore. Accumulation of a monolayer shrinks the diameter to $D_p - 2t_m$, lowering the surface area from $\pi L_p D_p$ by $2\pi L_p t_m$. However, agreement with measured PSDs cannot be achieved with this model. The problem is appreciably worse if the porosity is slit-shaped. Monolayer formation decreases the pore diameter, and its volume, but the surface area is unchanged. A second possible mechanism that may be operative is associated with pore blocking or attenuation events analogous to those depicted in Fig. 4, but occurring in the interior of the pore. We assume a normally distributed variability in the diameter around the measured pore diameter D_p down the length, denoted σ_{atten}. The probability that blocking might occur, $P_{block}(D_p)$, is proportional to the probability that the pore diameter is less than or equal to $2t_m$. This therefore yields:

$$P_{blocked}(D_p) = \frac{A([HF])}{\sigma_{atten}\sqrt{2\pi}} \int_{-\infty}^{2t_m} \exp\left(\frac{-[D - D_p]^2}{2\sigma_{atten}^2}\right) dD = \frac{A([HF])}{2}\left[1 + \mathrm{erf}\left(\frac{2t_m - D_p}{\sqrt{2}\sigma_{atten}}\right)\right] \quad (5)$$

The term $A([HF])$ is the constant of proportionality. This will also subsume any small corrections associated with slit versus cylindrical geometry and therefore this approach is applicable regardless of the underlying pore geometry. We have derived this term explicitly in previous work,[11] but its exact form is not particularly instructive here and will not be discussed further. However, it has been shown to be a function that increases with HF exposure and its role is to account for the fact that a blocking event becomes increasingly likely as more adsorbate deposits on the alumina surface. The pore length of the secondary alumina, L_s, may be calculated as $L_s = L_p P_{blocked}(D_p)$, and the new pore surface area computed from this perturbed pore length.

While this model is significantly more complex than a monolayer-only model, it provides exceptionally good accuracy. In instances where HF exposure is low, and PSD changes slight, monolayer or shrinking core-based models can lead to reasonable PSD reproductions. However, extremely poor fitting is found in general (see Fig. 5). On the other hand, extremely faithful reproductions of fluoride-dosed materials can be made over a wide range of fluoride loadings in both laboratory experiments and in industrial secondary aluminas (Fig. 6). It is important to note that we do not observe any of the pore shrinkage recently noted by Dando and Lindsay.[22] This may indicate that there may be two mechanisms operating. However, given the range of materials we have considered both here and in previous studies,[11–13,23–25] and the fact that models such as those shown in Fig. 5 do not, when examined in detail, demonstrate the sorts of shifts that Dando and Lindsay observe,[22] this suggests that it is also possible that the PSD changes they observe may be associated with a different deposition product. These possibilities will make intriguing future studies.

DISCUSSION

Previous work[21] on HF capture in dry scrubbing has focused on determining monolayer thickness t_m of the adsorbate on the alumina surface. These studies have implicitly assumed a shrinking-core model of a cylindrical pore that the results above have demonstrated does not comport with observation. However, the thickness of the adsorbate phase is still an important parameter. Our earlier results demonstrate that small pores are ineffective in fluoride return to the reduction cell through the secondary alumina. The blocking of pores, removing useful surface area, is an obvious possible mechanism to describe this phenomenon, as the smallest pores will be the most susceptible. The pore partitioning/attenuation model provides two independent estimates of t_m for a given alumina. The first is determined when fitting the partitioning between kinetically inaccessible and surface blocked pores (Eq. 4), the second in determining the new pore length after attenuation (Eq. 5). In a previous study, we reported an average value[11] of $t_m = 0.74 \pm 0.16$ nm. This was determined over a range of very different aluminas similar to those depicted in Fig. 6 subject to a considerable variation in fluoride loadings from both industrial and laboratory fluoride sources. The low error demonstrates the consistency of these values despite the varied alumina and fluoride source conditions. This indicates that this parameter is fundamental to the underlying chemistry and not simply a fitting artefact. This value is also in excellent agreement with previously determined estimates of 0.65–0.85 nm.[21]

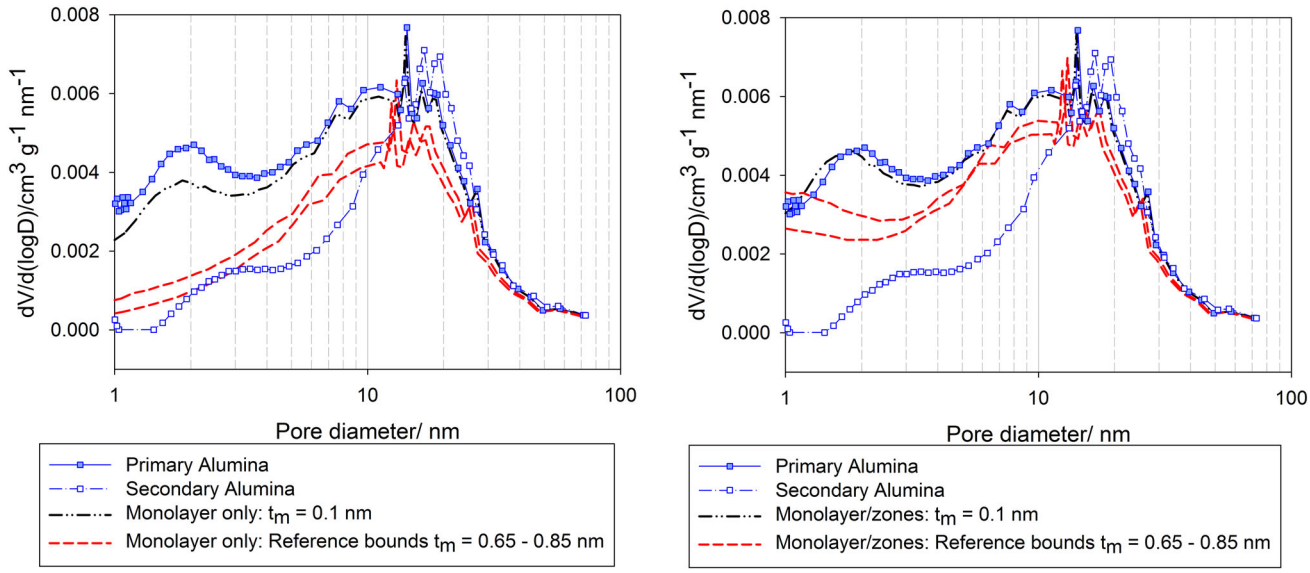

Fig. 5. PSD reconstruction results of a saturated alumina (laboratory-dosed with anhydrous HF) based on monolayer formation, with thickness derived in Ref. 21. Cylindrical pores are assumed (in the text we demonstrate that slit pores do not reveal any significant perturbation in the surface area based PSD). The plot on the left shows application of a monolayer on all pores, whereas on the right pore partitioning based on diffusion and pore blocking events (see Eqs. 2–4) is also considered. In general, surface area loss by core shrinkage cannot explain PSD shifts.

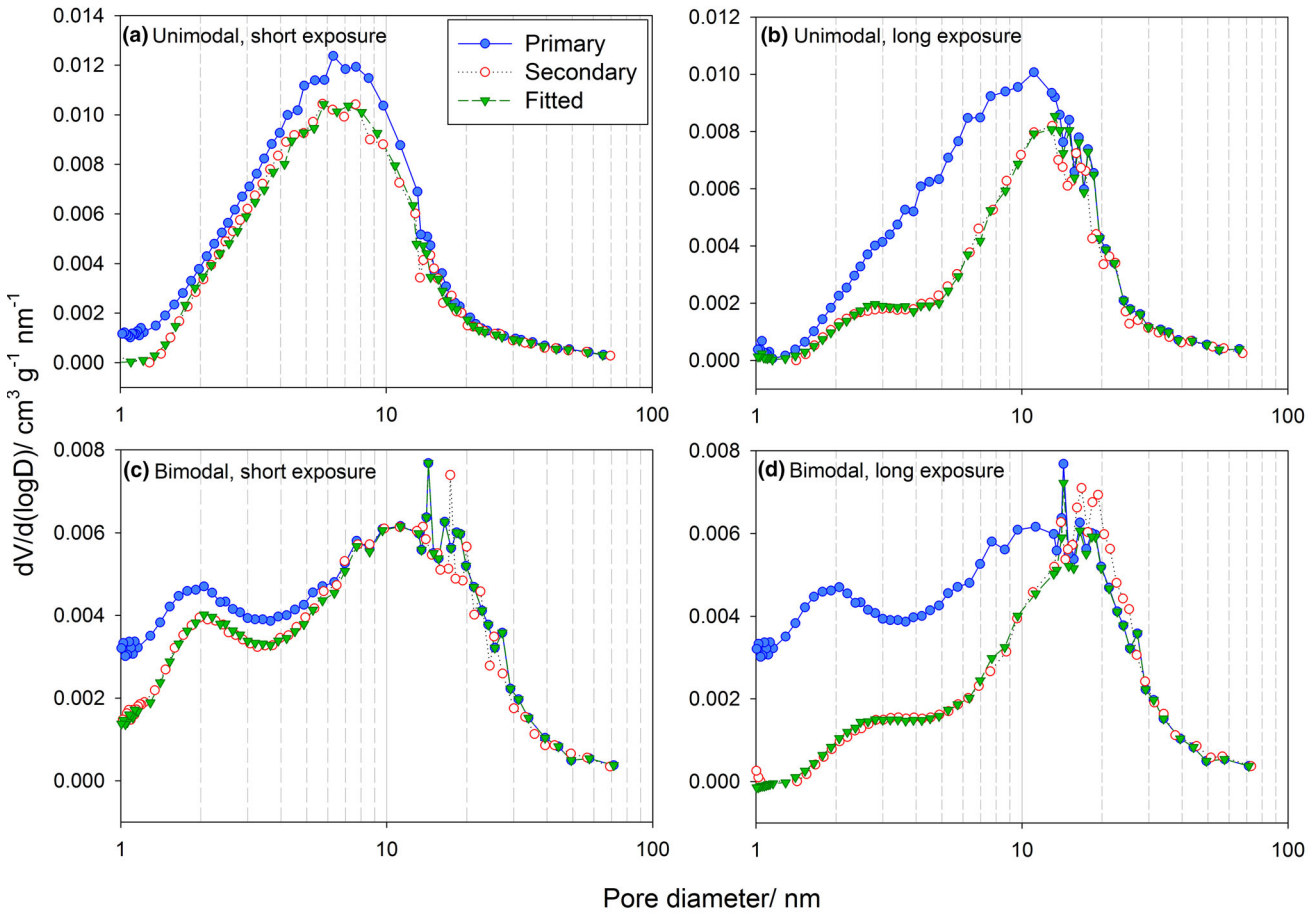

Fig. 6. PSD changes, both measured and fit, for (top) unimodal and (bottom) bimodal aluminas for (left) short and (right) long HF exposures. Short exposure changes are indistinguishable from those induced in an industrial GTC. Fitting results are derived assuming pore partitioning based on kinetic accessibility and pore blocking, and pore attenuation rather than core shrinkage.

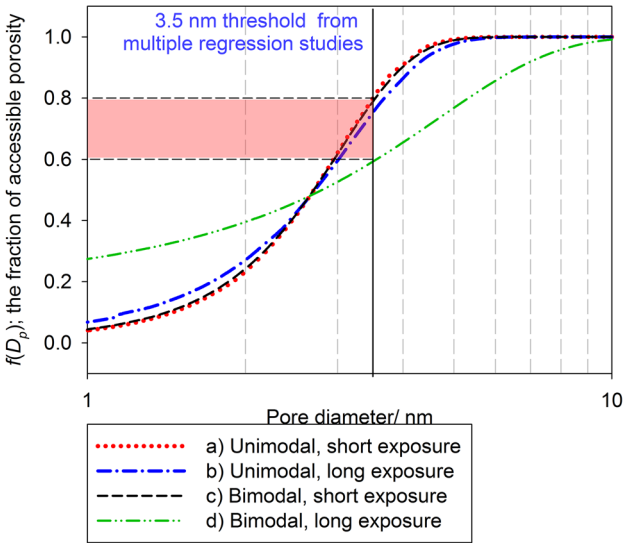

Fig. 7. Effective HF diffusivities as extracted from PSD fittings depicted in Fig. 6; see Eq. 2.

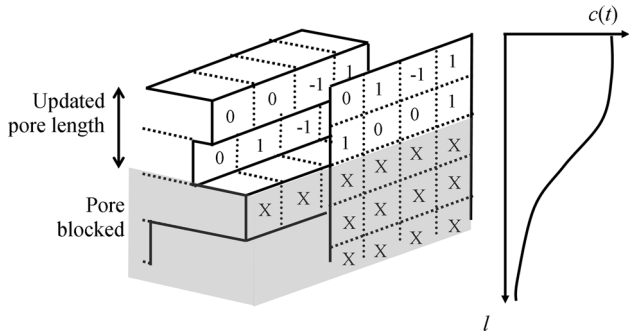

Fig. 8. Schematic depicting the concepts behind a revised molecular dynamics-like approach to PSD reconstruction. Pores, of variable (normally distributed) diameters are divided into reactive cells that are considered as matrix entries. These are randomly assigned '0' (unreactive) or '1' (reactive to HF) initially. Sites for adsorption are randomly chosen using a time-evolving HF concentration profile as a probability distribution. If adsorption can occur, the cell is designated with '−1' and if blocking criteria are met all cells at this length and below are rewritten with '*X*' denoting blocking. The pore length is updated accordingly.

However, restricted access due solely to pore blocking implies that the effective fluoride carrying capacity should be in porosity > 1.48 nm ($2t_m$). This in turn suggests that $XsAlF_3$ multiple regression models (Results A) should deliver the best fit when using PSD (≥1.48 nm) as a predictor. However, Fig. 2 demonstrates that the smallest pore which effectively captures fluoride is at least twice as large as that. Therefore, an additional mechanism beyond simple pore blocking must be responsible for limiting HF capture. The most likely cause based on our model construction is some form of kinetic exclusion from the pores. We can go some way to confirming this by examining the diffusion-related parameters we fit during PSD reconstructions, defined by Eq. 2 and demonstrated qualitatively in Fig. 3. The ERFs, partitioning accessible from kinetically hindered porosity, are plotted in Fig. 7 for the fitting depicted in Fig. 6. All large pores are completely accessible, $f(D_p) = 1$, with increasingly small pores becoming more difficult to access. Materials begin to exhibit appreciable losses of accessibility, on the order of 20%–40% at 3.5 nm. This is in excellent agreement with the results displayed in Fig. 2 displaying fluoride carrying capacity.

These results, taken together, provide very strong evidence that diffusion effects, and not simply pore blocking, must play the decisive role in determining HF capture. This therefore requires that useful surface area be associated with pores significantly larger than one may predict on the basis of the small size of the HF molecule.

The diffusion mechanism is not considered in these models. However, preliminary results[24] from a more refined procedure allow us to more explicitly explore this process. Pore geometries determined pore-by-pore from experimental isotherm data are used to produce a matrix representing all possible adsorption sites in the pore. Each cell in the pore/entry in the matrix is initially assigned a value of 0 or 1 to indicate if the site cannot be occupied or is reactive to HF, respectively (see Fig. 8). These are a function of the surface chemistry, with residual hydroxide groups or more basic oxide moieties presumably representing the reactive sites. The simulation then proceeds along a simplified molecular dynamics-like approach. Individual HF strikes with the pore wall are considered with a strike site chosen at random using a time-evolving concentration profile as a probability distribution. If adsorption can occur (i.e., an occupiable site is chosen) the cell is rewritten with a '−1'. Blocking is then checked; if all sites in the row are occupied on both walls, and the pore walls at this row are within ~$2t_m$, blocking has occurred. These, and all cells at lower lengths, are rewritten with '*X*" to designate inaccessibility, and the pore length is modified to account for shortening. This continues until all HF molecules have been considered, with this number a function of inlet concentration and exposure duration. This process is iterated over all pore diameters, and the PSD reconstructed using the modified pore lengths.

The power of this approach is that diffusion models can be examined explicitly. The concentration profile, from which one derives the probability that an HF strike will occur at l_p along the pore length, is given by:

$$c(l,t) = c_0\left[1 - \mathrm{erf}\left(\frac{l}{\sqrt{4\bar{D}_{\mathrm{tot}}(D_p)t}}\right)\right] \qquad (6)$$

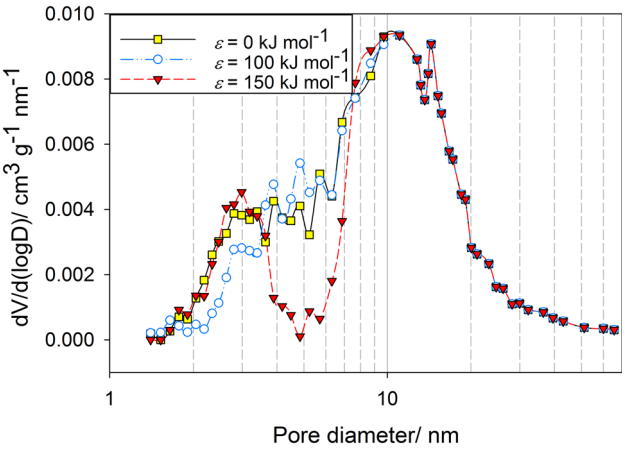

Fig. 9. Simulated PSDs as a function of the surface diffusion barrier parameter ε; see Eq. 9.

The total diffusion coefficient, $\breve{D}_{\mathrm{tot}}$, is a function of pore diameter; note the accent used to distinguish diffusivities $\breve{D}$ from pore diameters D. It is in this way that different diffusion models may be explored.

There are two models likely applicable here. The first is Knudsen diffusion, a variant on conventional molecular diffusion recognizing that, in narrow pores, the mean free path is the pore diameter. This diffusion coefficient, incorporating the molecular root-mean-square velocity v_{rms}, is given by:

$$\breve{D}_{\mathrm{knudsen}} = \frac{1}{3} v_{\mathrm{rms}} D_{\mathrm{p}} \tag{7}$$

Knudsen diffusion is active in pores $D_{\mathrm{p}} \sim 100$ nm and narrower,[26] with diffusivity decreasing with pore diameter. A second model of diffusivity is surface diffusion. Here, new mechanisms become important, such as overlapping of potential energies emanating from the wall surfaces introducing additional attractions with the adsorbate.[27] This results in an additional non-bonding attraction that forces an adsorbate to jump from site to site along the pore length, rather than freely drifting. This is given by:

$$\breve{D}_{\mathrm{config}} = \frac{1}{Z} v_{\mathrm{rms}} \alpha \exp\left(\frac{-E_{\mathrm{a}}(D_{\mathrm{pore}})}{RT}\right) \tag{8}$$

The term α gives the jump distance, with Z surrounding sites to which HF may jump. The key feature is that this is an activated process, dramatically slowing diffusion (by several orders of magnitude) relative to Knudsen diffusion.[27] Study into zeolites indicates that this regime is initiated in pores 1–5 nm in diameter;[26] the 3.5 nm threshold advocated here falls squarely in this range.

While the above is highly suggestive of a surface diffusion process causing HF exclusion, our models can demonstrate this explicitly. We assume the following total diffusivity and energy dependence on D_{pore} (Eq. 8):

$$\breve{D}_{\mathrm{tot}}^{-1}(D_{\mathrm{p}}) = \breve{D}_{\mathrm{knudsen}}^{-1} + \breve{D}_{\mathrm{config}}^{-1}; E_{\mathrm{a}}(D_{\mathrm{p}}) = \frac{\varepsilon}{D_{\mathrm{p}}^2} \tag{9}$$

This model of energy is not necessarily the most physically reasonable but gives the correct phenomenology: increasing barrier in ever smaller pores. Results of model simulations as a function of the parameter ε are given in Fig. 9. With $\varepsilon = 0$, we are in a purely Knudsen regime. It is possible to demonstrate that Knudsen diffusion cannot accurately describe the time-dependent changes observed as alumina is dosed,[24,25] indicating that surface diffusion must be active. Further, the energy parameter ε must be fine-tuned in order to describe the observed changes correctly, given the unreasonable PSD changes when the barrier is set too high (see $\varepsilon = 150$ kJ mol^{-1}; Fig. 9). This therefore indicates that these reconstructions will allow us to explore the energetics of pore wall chemistry, providing a powerful tool to study the alumina surface. The initial population of "0"'s and "1"'s (Fig. 8) will also provide insights into the role of alumina surface chemistry.

CONCLUSION

The results of recent studies undertaken by our group have led to several conclusions that have a tangible impact on predicting the nature of fluoride cycling in the smelting process. First, from data taken exclusively from an operating smelter, a pore diameter threshold of 3.5 nm is identified below which the pores are ineffective in fluoride return through HF capture. We have previously demonstrated that this affects the stack emissions,[13] and also influences the fluoride balance of the pot. We have also linked this to energy efficiency.[6] This indicates that the BET SSA, as reported on alumina specification sheets, is not ideal in predicting scrubbing or fluoride return efficiency, as this method necessarily includes this small pore surface area. Rather, the authors advocate a BJH-based estimate, requiring PSD knowledge, where pores ≤3.5 nm are explicitly omitted from the surface area. We note that current technology may make alumina quality concerns secondary. However, trends to decrease energy consumption[28] look to utilizing every available means to gain every bit of energy efficiency, and alumina quality is useful here. A close examination of the fundamental processes is therefore needed. Further, these insights will be invaluable in meeting future challenges. For example, phenomena such as low voltage anode effects[29] indicate alumina solubility is increasingly problematic, particularly as cells get larger. A shift to lower degrees of calcination may be one means to aid solubility, but our studies demonstrate that we cannot indefinitely lower this calcination degree with the expectation that the increased SSA will compensate for the increased emissions. The pore diameter

threshold advocated here represents a fundamental limit that GTC operations cannot circumvent. This may also become a problem in distributed pot suction methods for raw gas treatment;[28] the lower gas volume is associated with higher HF concentrations and temperatures, the latter both effectively "shrinking" the GTC bringing alumina quality back to prominence. These future trends may well benefit from knowing the "true" accessible SSA, with the BJH (<3.5 nm) method a direct means of achieving this.

PSD reconstructions of aluminas after the dry-scrubber reveal insights into the fundamentals of this process. We have demonstrated that surface area loss is not due to mono/multilayer formation (a shrinking core model), but rather due to pore shortening, a consequence of blocking along the pore length. From this, we have extracted a monolayer thickness (the size of the hydroxyfluoride phase formed on reaction) of 0.74 ± 0.16 nm, in good agreement with previous results.[21] This indicates that pore blocking alone cannot be responsible for the slowed uptake as this only accounts for pores smaller than $2t_m = 1.48$ nm. More sophisticated models demonstrate that this is very likely controlled by surface diffusion. This, and the model input requiring population of sites with accessible or inaccessible regions, indicates that a strong surface chemistry component is active in dry scrubbing. This may allow for some degree of tuning around which improved scrubbing performance could be obtained, and work is proceeding towards this objective.

REFERENCES

1. S. Meenakshi and R.C. Maheshwari, *J. Hazard. Mater.* 137, 456 (2006).
2. S. Ayoob and A.K. Gupta, *Crit. Rev. Environ. Sci. Technol.* 36, 433 (2006).
3. V. Søyseth, J. Kongerud, P. Broen, P. Lilleng, and J. Boe, *Arch. Dis. Child.* 73, 418 (1995).
4. P. Ernst, D. Thomas, and M. Becklake, *Am. Rev. Respir. Dis.* 133, 307 (1986).
5. S.C. Martin and C. Larivière, *J. Occup. Environ. Med.* 56, S33 (2014).
6. G.J. McIntosh, J.B. Metson, P. Lavoie, T. Niesenhaus, T. Reek, and L. Perander, *Light Metals 2016* (John Wiley & Sons, Inc., Hoboken, NJ, 2016), p. 417.
7. A.R. Gillespie, M.M. Hyland, and J.B. Metson, *JOM* 51, 30 (1999).
8. S. Brunauer, P.H. Emmett, and E. Teller, *J. Am. Chem. Soc.* 60, 309 (1938).
9. L.M. Perander, Z.D. Zujovic, T.F. Kemp, M.E. Smith, and J.B. Metson, *JOM* 61, 33 (2009).
10. L.M. Perander, M.A. Stam, M.M. Hyland, and J.B. Metson, *Light Metals 2011* (John Wiley & Sons, Inc., Hoboken, NJ, 2011), p. 285.
11. G.J. McIntosh, G.E.K. Agbenyegah, M.M. Hyland, and J.B. Metson, *Langmuir* 31, 5387 (2015).
12. G.E.K. Agbenyegah, G.J. McIntosh, M.M. Hyland and J.B. Metson, Australasian Aluminium Smelting Technology Conference, Dubai, United Arab Emirates, 2014.
13. G.J. McIntosh, J.B. Metson, T. Niesenhaus, T. Reek, and L.M. Perander, *JOM* 66, 2272 (2014).
14. M. Iffert, M. Kuenkel, M. Skyllas-Kazacos, and B. Welch, *Light Metals* (John Wiley & Sons, Inc., Hoboken, NJ, 2006), p. 195.
15. E.P. Barrett, L.G. Joyner, and P.P. Halenda, *J. Am. Chem. Soc.* 73, 373 (1951).
16. D.K. Jaiswal, A. Kumar, and R.R. Yadav, *J. Water Resour. Prot.* 3, 76 (2011).
17. C. Zoppou and J.H. Knight, *Appl. Math. Model.* 23, 667 (1999).
18. N.R. Dando, *Light Metals* (The Minerals, Metals & Materials Society, Warrendale, PA, 2005), p. 133.
19. A.R. Gillespie, Ph.D. Thesis, The University of Auckland, 1997.
20. R.G. Haverkamp, J.B. Metson, M.M. Hyland, and B.J. Welch, *Surf. Interface Anal.* 19, 139 (1992).
21. W.D. Lamb, *Light Metals* (The Metallurgical Society of AIME, Warrendale, PA, 1978), p. 425.
22. N.R. Dando and S.J. Lindsay, *Light Metals 2016* (John Wiley & Sons, Inc., Hoboken, NJ, 2016), p. 527.
23. G.J. McIntosh, G.E. Agbenyegah, and J.B. Metson, *CiNZ* 79, 36 (2015).
24. G.J. McIntosh, G.E.K. Agbenyegah, and J.B. Metson, Mechanisms of Diffusion in Porous Media Based on Modeling of Time Resolved HF Dosing of Alumina., *Manuscript in Preparation* (2016).
25. G.E.K. Agbenyegah, G.J. McIntosh, M.M. Hyland, and J.B. Metson, *Light Metals 2016* (John Wiley & Sons, Inc., Hoboken, NJ, 2016), p. 519.
26. J.D. Way and D.L. Roberts, *Sep. Sci. Technol.* 27, 29 (1992).
27. J. Xiao and J. Wei, *Chem. Eng. Sci.* 47, 1123 (1992).
28. M. Segatz, J. Hop, P. Reny, and H. Gikling, *Light Metals 2016* (John Wiley & Sons, Inc., Hoboken, NJ, 2016), p. 301.
29. D.S. Wong, P. Fraser, P. Lavoie, and J. Kim, *JOM* 67, 342 (2015).